

# Chaos assisted tunnelling with cold atoms

A. Mouchet<sup>1\*</sup>, C. Miniatura, R. Kaiser<sup>2†</sup>, B. Grémaud, D. Delande<sup>3‡</sup>

<sup>1</sup>*Laboratoire de Mathématiques et de Physique Théorique (CNRS UPRES-A 6083). Avenue Monge, Parc de Grandmont 37200 Tours, France.*

<sup>2</sup>*Institut Non Linéaire de Nice (CNRS UMR 7618), 1361, route des Lucioles, Sophia Antipolis, F-06560 Valbonne, France.*

<sup>3</sup>*Laboratoire Kastler-Brossel (CNRS UMR 8552), Université Pierre et Marie Curie, 4, place Jussieu, F-75005 Paris, France.*  
(October 29, 2018)

In the context of quantum chaos, both theory and numerical analysis predict large fluctuations of the tunnelling transition probabilities when irregular dynamics is present at the classical level. We consider here the non-dissipative quantum evolution of cold atoms trapped in a time-dependent modulated periodic potential generated by two laser beams. We give some precise guidelines for the observation of chaos assisted tunnelling between invariant phase space structures paired by time-reversal symmetry.

PACS : 05.45.Mt Semiclassical chaos (quantum chaos)  
05.60.Gg Quantum transport  
32.80.Qk Coherent control of atomic interactions with photons  
05.45.Pq Numerical simulations of chaotic models

## I. INTRODUCTION

During the seventies and the eighties, it became gradually clear that classical Hamiltonian chaos profoundly affects the temporal evolution and the spectral properties of the corresponding quantum system as compared to the integrable case [1]. Some of these features (dynamical localization, scars of periodic orbits [2], etc) share striking similarities with concepts originating from condensed matter such as weak and strong localization [3]. In fact these phenomena can be recast in terms of wave transport in disordered media, (quasi)-randomness being of statistical or dynamical origin. In this context, it is important to understand the mechanisms underlying a key feature of wave propagation which has no classical analog: tunnelling.

Tunnelling refers to any wave process which is classically forbidden to *real* solutions of Hamilton equations. For one-dimensional (1D) autonomous systems, it is well known that the quantum tunnelling probability through an energetic barrier can be evaluated semiclassically with the help of classical *complex* solutions of Hamilton equations [4,5]. The direct generalization of this procedure to higher dimensional systems is straightforward for separable dynamics but is already subtle for still integrable, but no longer separable, dynamics [6,7]. In the generic case of chaotic dynamics, it even proves extremely hard to handle and the situation, until recently, seemed hopeless. This is so because, in the presence of chaos, the analytical and topological properties of the classical *complexified* phase space are far from trivial. During the last ten years however, theoretical and numerical investigations on autonomous 2D and time-dependent 1D Hamiltonians systems have started to highlight some mechanisms [6–12] and much insight has been gained on the influence of such classical non-separable dynamics. Experimental evidence of such mechanisms, which is still lacking, would be of great interest especially in the light of the subtle interplay between interferences and disorder.

In this paper, we consider 1D time-dependent dynamics, one of the simplest case where irregular motion can appear, and we study chaos assisted tunnelling. Our effective Hamiltonian model, which is derived from an experimentally achievable situation, exhibits three main properties. First, its classical dynamics is time-reversal invariant. Second it is controlled by a single real external parameter  $\gamma$  (for  $\gamma = 0$  the dynamics is integrable and chaos develops more and more in phase space as  $\gamma$  is increased). Third, there exists in phase space, for a whole continuous range of  $\gamma$ , a pair of stable islands  $\mathcal{I}_+$  and  $\mathcal{I}_-$  which are time reversed images of each other. By stable islands we mean the set of regular classical trajectories in phase space which stay near a stable equilibrium point or near a stable periodic orbit of the system. In this case, no real classical orbit started in one of these islands can go into the other one. However, the quantum dynamics of a wave-packet, initially prepared in one island, will display a periodic behavior. The wave-packet jumps from one island to its time reversed image [13]. In the quantum spectrum this tunnelling process appears via the existence of non degenerate energy doublets whose splitting give the inverse of the tunnelling

---

\*mouchet@celfi.phys.univ-tours.fr

†miniat,kaiser@inln.cnrs.fr

‡gremaud,delande@spectro.jussieu.fr

time between  $\mathcal{I}_+$  and  $\mathcal{I}_-$ . Varying  $\gamma$  slowly modifies the geometry of the islands themselves. The crucial point is that it will drastically change the classical dynamics for some initial conditions lying between the islands. For  $\gamma$  small enough, the chaotic layers are too small to play a significant role at  $\hbar$  scales and hence cannot influence the quantum behaviour of the system which is essentially still regular. For larger values, but still before the stable islands are completely destroyed, there is a chaotic regime where varying  $\gamma$  or  $\hbar$  (by  $\hbar$  we mean here Planck's constant divided by some typical classical action) alone induces large fluctuations, on several orders of magnitude, of the doublet splittings around their mean value. This in turn means large fluctuations of the tunnelling periods. These wild fluctuations induced by small changes of any parameter are a signature of the so-called ‘‘chaos assisted tunnelling’’ regime. It has been extensively studied both theoretically and numerically in the situation described above [8–11] but has not been yet observed in real experiments, the main reason being its extreme sensitivity to small changes in the classical dynamics. Any *uncontrolled* variation of  $\gamma$ , be it noise or dissipation, will dramatically swamp or destroy the signal. The observation of this highly fluctuating tunnelling regime thus requires both an accurate control of the dynamics, of the preparation of the initial state and of the analysis of the final state.

Atom cooling techniques [14] provide systems which fulfill all these requirements. They allow an accurate manipulation and control of internal and external degrees of freedom and are now a useful tool to produce situations where the wave character of the atomic motion is essential [15]. A great variety of potentials can be produced to influence the atomic motion, be it by means of inhomogeneous magnetic fields, material gratings or laser light. Optical lattices with crystalline or quasi-crystalline order [16–18] can be easily produced where atoms mimic situations usually encountered in condensed matter [19,20]. Dissipation (spontaneous emission and atom-atom interaction) is easily controlled and coherence times of the order of 10 ms can be achieved. This is why cold atoms are a unique tool to study transport properties of waves, be it quantum chaos [21] or weak localization [22,23].

The general organization of this paper is the following. In section II we explain the origin of the effective Hamiltonian for the experimental situation under consideration. In section III we study the corresponding classical dynamics and show why this effective Hamiltonian is relevant for chaos assisted tunnelling. In section IV we quickly review some of the usual theoretical techniques when dealing with both space and time periodic quantum dynamics. We also illustrate how some quantum spectral properties have a natural classical interpretation. In section V we show, with the help of numerical experiments, how chaos assisted tunnelling arises in our system and then explain how to observe it in a real experiment. Section VII is devoted to some concluding remarks.

## II. EFFECTIVE HAMILTONIAN

### A. Light shifts

The very basic physical mechanism underlying our forthcoming discussion is the following: when an atom is exposed to monochromatic light, its energy levels are shifted by the interaction. These level shifts originate from the polarization energy of the atom in the incident light field and are called the light shifts [24]. In the dipolar approximation, they only depend on the field intensity value at the center-of-mass position of the atom. If the field intensity is space-time dependent, then a moving atom will experience dipolar forces: inhomogeneous light shifts act as potentials and alter the center-of-mass motion of the atom. By appropriately tailoring the space-time dependence of the light field, one can then produce a great variety of potentials for the external atomic motion as evidenced by the atom cooling industry. Note, however, that the atom-light interaction is also responsible for a dissipative phenomenon (real absorption of a photon followed by spontaneous emission) which shortens the temporal coherence of the atomic wave function. By using a laser light far detuned from any atomic resonance, it is possible to control this stray phenomenon and maintain it at a reasonably low rate.

In the following, we shall describe a simple physical situation for atoms where chaos assisted tunnelling should show up.

### B. Experimental configuration

Although the internal structure (hyperfine Zeeman sub-levels) are of major importance in the atom cooling techniques, we will here for simplicity model the atom by a two-level system (as indeed, only one optical transition usually governs the dynamics). We consider a dilute sample of identical (but independent) two-level atoms propagating in the light field configuration created by two monochromatic standing waves with frequencies  $\omega_{\pm} = \omega_L \pm \delta\omega/2$  where  $\delta\omega \ll \omega_L$ . We denote by  $|g\rangle$  and  $|e\rangle$  the ground-state and the excited state of each atom, these levels being connected by an electric dipole transition of angular frequency  $\omega_{at}$  and width  $\Gamma$ . All atoms are supposed to be initially

prepared in their ground state. Each standing-wave is produced along the  $x$  axis by two counter-propagating laser beams and we suppose all fields to be linearly polarized along the  $z$  axis (see figure 1). After a suitable choice of space-time origin, the total electrical field strength is

$$E(x, t) = [E_+ \cos(\omega_+ t) + E_- \cos(\omega_- t)] \cos(k_L x) \quad (1)$$

where  $E_{\pm}$  are the field strengths of the two standing-waves. At this point we have neglected the difference in wave-vectors of the standing-waves. For this to hold, it is sufficient to assume that the atomic sample size is small enough. Typically, the difference in the  $k$  vectors will be of the order of  $10^{-9}$  or less (see below), so that this requires the atomic cloud to be smaller than typically few kilometers, which is amply satisfied in a standard magneto-optical trap.

### C. Dimensionless effective Hamiltonian

The effective Hamiltonian which describes the atomic motion is derived in appendix A under some common and well-controlled approximations. It acts in the Hilbert space of a one-dimensional system which is simply the  $x$  component (position) of the center of mass of the atom (which means that the internal degree of freedom as well as the  $y$  and  $z$  coordinates can be eliminated, see Appendix). It reads:

$$H = \frac{p_x^2}{2M} - V_0 \cos(2k_L x) [\theta + \cos(\delta\omega t)] \quad (2)$$

where  $V_0 \stackrel{\text{def}}{=} -\hbar\Omega_+\Omega_-/8\delta_L$  and  $\theta \stackrel{\text{def}}{=} (\Omega_+/2\Omega_-) + (\Omega_-/2\Omega_+)$ , with  $\delta_L = \omega_L - \omega_{at}$  the detuning with respect to the atomic frequency and  $\Omega_{\pm} = dE_{\pm}/\hbar$  ( $d$  being the atomic dipole strength). Without loss of generality we will assume  $V_0$  to be positive since, if  $V_0$  is negative, it is sufficient to shift  $x$  by  $\pi/2k_L$  to recover this case.

In the following, it will prove convenient to work with dimensionless quantities. Rescaling quantities through  $\tau \stackrel{\text{def}}{=} \delta\omega t$ ,  $q \stackrel{\text{def}}{=} 2k_L x$ ,  $p \stackrel{\text{def}}{=} (2k_L/M\delta\omega)p_x$ ,  $\gamma \stackrel{\text{def}}{=} (4k_L^2/M\delta\omega^2)V_0$  and  $H_{\text{eff}} \stackrel{\text{def}}{=} (4k_L^2/M\delta\omega^2)H$ , then yields the dimensionless effective Hamiltonian:

$$H_{\text{eff}} = \frac{p^2}{2} - \gamma (\theta + \cos\tau) \cos q. \quad (3)$$

Such an Hamiltonian describes the dynamics of a periodically driven pendulum. The associated quantum canonical commutation relation is  $[q, p] = i\hbar_{\text{eff}}$  and we get  $\hbar_{\text{eff}} = 8\omega_R/\delta\omega$  where  $\omega_R = \hbar k_L^2/2M$  is the atomic recoil frequency and  $\delta\omega$  is the beating frequency between the laser waves.

Such an effective Hamiltonian clearly exhibits two of the three properties mentioned in the introduction: the corresponding classical dynamics is governed by a single classical parameter, the dimensionless coupling strength  $\gamma$ , and is invariant under time-reversal symmetry  $(p, q, \tau) \mapsto (-p, q, -\tau)$ . It is worth mentioning that the semiclassical limit  $\hbar_{\text{eff}} \rightarrow 0$  is realized here by increasing the beating frequency  $\delta\omega$  between the two laser waves.

With our field configuration, only  $\theta \geq 1$  can be achieved. As a slight generalization, we extend the range of  $\theta$  to any positive value since one can design other field configurations where  $\theta \leq 1$  occurs. For example,  $\theta = 0$  yields the Hamiltonian studied in [13] in a different context.

### D. Orders of magnitude

Let us give some typical experimental parameters. For Rubidium atoms, the atomic parameters are  $M = 85$  amu,  $\lambda_{\text{at}} = 2\pi c/\omega_{\text{at}} = 0.78 \mu\text{m}$ ,  $\Gamma/2\pi = 6$  MHz,  $\omega_R/2\pi = 3.8$  kHz and saturation intensity  $I_{\text{sat}} = 1.6$  mW/cm<sup>2</sup>. Using far-detuned laser beams ( $2\delta_L/\Gamma = 10^4$ ) focussed down to  $500 \mu\text{m}$  (power 100 mW), with a beating frequency  $\delta\omega/2\pi = 60$  kHz, lead to  $\gamma = 0.4$  and  $\hbar_{\text{eff}} = 0.05$ . With such values, spontaneous emission can be neglected up to times of the order of few ms. It is worth noticing the tiny energies which come into play ( $V_0 \sim 5$  eV), by several orders of magnitude smaller than the typical ones for mesoscopic systems.

## III. CLASSICAL DYNAMICS

## A. Poincaré surface of section

A Poincaré surface of section provides the usual tool for visualizing the classical dynamics [25]. As  $H_{\text{eff}}$  is  $2\pi$ -periodic both in time and space, this surface of section simply consists in the whole phase space itself (which has the topology of a cylinder) where trajectories  $(p(\tau), q(\tau))$  are seen stroboscopically at every time period  $2\pi$ . In the following, without any substantial loss of generality, we will restrict our analysis to the case  $\theta = 1$  which is easily experimentally achieved when the standing waves have the same field strengths.

Figure 2 shows stroboscopic plots of phase space orbits for different  $\gamma$ 's. For  $\gamma = 0$ ,  $p$  is a constant of motion, so that the system is integrable and the surface of section is composed of horizontal lines. For  $\gamma$  weak enough (fig. 2-a), the orbits remain confined to invariant curves. These invariant curves stratify the whole phase space and the dynamics appears regular. One can clearly see well separated stability islands, each being bordered by a separatrix. This is the situation encapsulated in the KAM theorem for near-integrable motion: although no globally-defined constants of motion exist, some invariant curves can still be constructed which order the dynamics. As  $\gamma$  is increased (fig. 2-b), some of more and more invariant curves are broken and chaotic layers start to spread around separatrices. These layers fill some portion of phase space but motion is still predominantly confined to invariant curves. Above some coupling threshold (fig. 2-c to 2-e), stochastic orbits invade phase space and the surviving stability islands are surrounded by a connected chaotic sea. This occurs for  $\gamma \sim 0.1$ . The phase space structure in this regime is typical of a mixed dynamics where regular orbits co-exist with stochastic ones. If  $\gamma$  is increased further (fig. 2-f), the stability islands disappear (or are too small to be seen at this scale) and one gets global chaos. We note however that, even in this situation, the chaotic portion of phase space is still bounded by invariant curves which means that chaos can only fully develop within some range of momentum  $p$ .

## B. Resonances

At this stage, let us rewrite the effective Hamiltonian as follows:

$$H_{\text{eff}} = H_0 + \gamma H_1 = \frac{p^2}{2} - \gamma \cos q - \frac{\gamma}{2} \cos(q + \tau) - \frac{\gamma}{2} \cos(q - \tau) \quad (4)$$

The physical interpretation of the various terms is rather simple: the two counter-propagating laser beams at frequency  $\omega_+$  create a stationary wave which, in turn, creates for the atom an effective optical potential proportional to the square of the modulus of the electric field in the standing wave, hence the  $\cos q$  dependence (it is actually rather  $1 + \cos q$ , but the constant term does not play any role in the dynamics). The same effective potential is due to the standing wave created by the two  $\omega_-$  counter-propagating beams. A pair of counter-propagating beams at frequencies  $\omega_+$  and  $\omega_-$  does not create a standing wave in the lab frame. However, in a frame sliding at constant velocity  $v_0 = (\omega_+ - \omega_-)c/2\omega_L$ , ( $=1$  in rescaled units) the two laser beams are shifted in frequency by Doppler effect and appear to have equal frequency, building another stationary wave and yet another effective optical potential. In the lab frame, this appears as a modulated optical potential moving at velocity  $v_0$ . By symmetry, there are two such effective potentials moving either to the right or to the left. These are the  $\cos(q \pm \tau)$  terms in the Hamiltonian.

This form of the Hamiltonian is in order to point out the perturbative terms which may be resonant with the unperturbed frequencies. When  $\gamma = 0$ , the system is integrable since we recover free motion:  $H_{\text{eff}}$  reduces to  $H_0 = p^2/2$  and  $(p, q)$  are exact action-angle variables. For  $\gamma > 0$ , the absence of any constant of motion generates chaos. Stroboscopic plots of phase-space trajectories are no more constrained to follow lines of constant  $H_0$  but generically fill densely a two dimensional volume in phase space. As long as  $\gamma$  is small enough, these volumes remain thin enough not to be distinguished from regular lines at the scale of finite precision of the measurements and/or the calculations (*cf.* figure 2-a). Nevertheless, for higher values of  $\gamma$ , some chaotic layers can be seen (*cf.* figure 2-b) between regular regions. They consist of portions of phase space where trajectories are exponentially sensitive on initial conditions. From classical first-order perturbation theory [25, chap. 2], we can infer that a term of the form  $A \cos(sq - r\tau)$ , where  $(s, r)$  are integers, will create a resonance of width  $\Delta p = 4\sqrt{A}$  around the point  $p = r/s$ . In our case,  $s = 1$  and there exist only three such resonances. They are located at  $p = 0$  ( $r = 0$ ) and at  $p = \pm 1$  ( $r = \pm 1$ ). This can be seen in figure 2 (a to e). For each resonance there exists one stable and one unstable periodic orbit with period approximately  $2\pi|r|$ . In the stroboscopic plot of the surface of section, they appear as a stable and unstable fixed points and give rise locally to the well-known phase-space portrait of a pendulum. In the following, we will denote by  $\mathcal{I}_0, \mathcal{I}_+, \mathcal{I}_-$  the three stable islands associated with  $r = 0, +1, -1$  respectively. The physical interpretation of these three resonances is simple: each resonance is associated with one of the modulated potentials (either static or moving) described above. For example, the fixed point at the center of the  $\mathcal{I}_+$  resonance is associated with a periodic

orbit where the atom moves at almost constant velocity  $v_0$ , being in fact trapped in the minimum of the moving optical potential. The other two components of the potential appear along this orbit as rapidly varying potentials which are adiabatically averaged to constant values. As the atom can be trapped in any of the 3 modulated potentials, we obtain three stable periodic orbits at the centers of the 3 resonance islands.

For  $\gamma$  small enough, the resonances are well separated and the motion is quasi-integrable. Chaos will develop when the resonances start to overlap. This is the celebrated Chirikov's overlap criterion [26] and its evaluation gives  $\gamma \simeq 0.1$  in our case. Thus chaos develops in phase-space regions where the kinetic energy term and the perturbation are of the same order of magnitude. Taking into account higher perturbation orders in  $\gamma$  will shift the position in phase-space of the previous resonances as well as the frequency around their stable points. For instance, it can be seen in figure 2-e that the stable island  $\mathcal{I}_+$  is centered on a point having a momentum slightly larger than +1. Perturbation terms of higher order will also introduce other resonances of smaller size. It is precisely the overlap of the infinite cascade of such resonances which gives rise to the chaotic layers. Nevertheless, Chirikov's criterion already gives a good order of magnitude for the onset of chaos. For higher  $\gamma$ , the previous three resonant islands of stability have shrunk inside a large chaotic sea and eventually disappear completely (*cf.* figure 2-f). Nevertheless revival of some stable islands can still be observed for some narrow windows of high  $\gamma$ 's. In our situation, chaos cannot invade the whole phase space but is bounded by regular coasts. This is so because chaos develops where resonances overlap. Sufficiently far away from the resonances, atoms move so fast that they experience an average time-independent potential. Then chaos is absent and one recovers (quasi)-free motion when  $|p| \gg 1$ .

### C. Typical classical phase space portrait in the chaos assisted tunnelling regime

The two resonant islands  $\mathcal{I}_\pm$ , when they exist, are related by a discrete symmetry: the time reversal invariance. As can be seen in figure 3, the atoms trapped in one island cannot classically escape from it: the boundaries of the islands play the role of a dynamical barrier which atoms cannot cross. Hence jumping from one island to the other is a classically forbidden process though it is expected to occur in quantum mechanics. This is precisely the tunnelling situation we are interested in. In fact, we will study the tunnelling between  $\mathcal{I}_+$  and  $\mathcal{I}_-$  for  $\gamma$  varying from 0.1 to 0.3 since, in that range, classical chaos may play a revealing role though the two stable islands still occupy a significant volume in phase space.

Note that, in the physical situation described by  $H_{\text{eff}}$ , tunnelling occurs in momentum coordinate instead of space coordinate as it is usually presented in standard textbooks. The denomination of "dynamical tunnelling" [27], refers to this situation. The reason for investigating this situation is that manipulation of cold atoms allows for a better control (preparation and detection) of momentum rather than position.

## IV. QUANTUM DYNAMICS

### A. Floquet-Bloch theory

When an autonomous Hamiltonian is spatially periodic, it is well known [28] that its spectrum is organized in energy bands  $E_n(k)$ . These bands are labelled by a set of integers, the band index  $n$ , and depend continuously on a set of real numbers, the Bloch numbers  $k$ . As  $E_n(k)$  and the associated eigenfunctions are periodic functions of the  $k$ 's, all the physical information is contained in the first Brillouin zone. For 1D-systems, it is simply the interval  $[-\frac{\pi}{Q}, \frac{\pi}{Q}]$ , where  $Q$  is the spatial period of the Hamiltonian.

When the Hamiltonian is time-periodic, with period  $T$ , the analogous of Bloch theory is Floquet theory [29–31]. The eigenvalues of the evolution operator  $U(\tau+T, \tau)$  over one period take the form  $e^{-i\epsilon T/\hbar_{\text{eff}}}$ . The  $\epsilon$ 's are  $\tau$ -independent real quantities which are called the quasi-energies of the system. Due to the time-periodicity, the quasi-energy spectrum as well as the associated eigenfunctions are now invariant under  $\epsilon \mapsto \epsilon + 2\pi\hbar_{\text{eff}}/T$ .

For  $H_{\text{eff}}$ , the application of Bloch and Floquet theorems with  $Q = T = 2\pi$  yields a spectrum made of quasi-energy bands  $\epsilon_n(k)$  where  $n$  goes over the whole set of integers (for a detailed derivation see appendix B). For brevity, we will define  $|n, k, \tau\rangle$  the ket at time  $\tau$  with Bloch angle  $k$ , with quasienergy  $\epsilon_n(k)$  and which is a solution of the Schrodinger's equation (following the notations of appendix B, we have set  $|n, k, \tau\rangle \stackrel{\text{def}}{=} |\psi_{\epsilon_n(k), k}(\tau)\rangle$ ). We will also define  $|n, k\rangle \stackrel{\text{def}}{=} |n, k, \tau = 0\rangle$ .

As it can be seen in figure 4, the band spectrum has the topology of a torus since it is both periodic in quasi-energy (with period  $\hbar_{\text{eff}}$ ) and in Bloch number (with period 1).

## B. Numerical calculation of the Floquet eigenstates

As derived in appendix B, the Floquet eigenstates can be obtained by diagonalization of the Floquet-Bloch operator,  $\tilde{K}$

$$\tilde{K}(\hat{p}, \hat{q}, \tau, k) = \frac{(\hat{p} + \hbar_{\text{eff}} k)^2}{2} - \gamma \cos \hat{q} (1 + \cos \tau) - i \hbar_{\text{eff}} \frac{d}{d\tau}, \quad (5)$$

with periodic boundary conditions both in time and space. The eigenvalues, which depend on the Bloch vector  $k$ , are the quasi-energies of the system. The band spectrum is symmetric with respect to the axis  $k = 0$  since the operator (5) is invariant under the transformation  $k \mapsto -k$  and  $p \mapsto -p$ . From the expression of the Floquet-Bloch operator and the boundary conditions, it is very natural to expand the eigenstates on a basis set composed of products of the type  $\phi_{lm}(\tau, q) = \exp(in\tau) \exp(imq)$  which automatically obey the periodic boundary conditions. In such a basis, the operator  $\tilde{K}$  has very strong selection rules, namely:

$$|\Delta n| \leq 1 \quad \text{and} \quad |\Delta m| \leq 1 \quad (6)$$

All matrix elements violating one of these selection rules is zero. Hence, the matrix representing the operator  $\tilde{K}$  in this basis is sparse and banded, and all matrix elements have simple analytical expressions. This is well suited for numerical diagonalization (powerful algorithms exist, for example the Lanczos algorithm). All the numerical results presented here use this method. We checked that the effect of the truncation of the basis is negligible: the size of the Floquet matrix is considered as sufficiently large when increasing it modifies the value of the quasi-energy on the scale of the numerical noise only, say  $10^{-15}$  in double precision. Not only this criterion is a proof of algorithmical convergence but also it is a safeguard against numerical discrepancies since we are looking for exponential small quantities.

## C. Husimi representation and classification of the quantum states

Classical dynamics is very illuminating when describing the states  $|n, k, \tau\rangle$ . In order to strengthen the correspondence between classical phase-space structures and quantum states, it is convenient to work with the Husimi representation of quantum states [32].

Such a representation associates to each quantum state  $|\psi\rangle$  a phase space function  $\psi^{\text{H}}(p, q)$  (where  $p$  and  $q$  are real numbers) defined by

$$\psi^{\text{H}}(p, q) \stackrel{\text{def}}{=} N_{\psi} |\langle z|\psi\rangle|^2 \quad (7)$$

where  $|z\rangle$  is the normalized coherent state corresponding to the complex number  $z = (q + ip)/\sqrt{2\hbar_{\text{eff}}}$ .  $N_{\psi}$  is a  $(p, q)$ -independent normalization factor. Because  $|z\rangle$  is a minimal gaussian wave packet with average momentum  $p$  and average position  $q$ , the Husimi function  $\psi^{\text{H}}(p, q)$  contains some information about the degree of localization of  $|\psi\rangle$  in phase space.

The minimal cell size in phase-space allowed by the Heisenberg inequalities is  $\hbar_{\text{eff}}$ . Let us see how classical phase space structures of typical size larger than  $\hbar_{\text{eff}}$  are mirrored at the quantum level. In figure 5 and 6 we have plotted some of the  $\epsilon_n(k)$  corresponding to the Hamiltonian (3) for specified fixed values of  $\gamma$  and  $\hbar_{\text{eff}}$ . Von Neumann and Wigner arguments [33] claim that, generically, no exact degeneracy can occur: one rather gets avoided crossings. Of course, this is relevant provided the minimal energy splitting is greater than the resolution in energy. Some Husimi functions are plotted in figure 5 and 6 (a to f) <sup>1</sup>.

---

<sup>1</sup>A technicality should be mentioned here:  $|u_{\epsilon, k}\rangle$  and  $|\psi_{\epsilon, k}\rangle$  obey some spatial boundary conditions which are lost when working with their Husimi representations, essentially because the coherent states do not fulfill themselves these properties. To deal with spatially (quasi-)periodic phase-space functions it is necessary to unfold the coherent states [34] into

$$|z, k\rangle \stackrel{\text{def}}{=} \sum_{m \in \mathbf{Z}} e^{imkQ} |z + mQ\rangle \quad (8)$$

In appendix B, it is shown that we have

$$v_{n,k} \stackrel{\text{def}}{=} \frac{1}{T} \int_0^T \langle n, k, \tau | \hat{p} | n, k, \tau \rangle d\tau = \frac{1}{\hbar_{\text{eff}}} \frac{\partial \epsilon_n}{\partial k}, \quad (10)$$

which generalizes the velocity theorem [28, Appendix E] to periodic time-dependent hamiltonians.

Figure 5-b shows an example of the Husimi representation of a state with sufficiently high average velocity to be alike a free eigenstate of  $H_0$ . Far from quasi-degeneracies it is localized in a narrow strip of width  $\Delta p \sim 2\pi\hbar_{\text{eff}}/\Delta q \sim \hbar_{\text{eff}}$  (since  $\Delta q$  covers  $2\pi$ ) and which is centered on one of the two classical phase space trajectories of energy about  $v_{n,k}^2/2$  (compare with figure 2-e). Its quasi-energy band (figure 5) is an arc of the parabola of the free motion but can hardly be distinguished from a straight line of slope  $v_{n,k}$  if  $k$  is restricted to one Brillouin zone. We will naturally call these states quasi-free states.

Some states have their Husimi functions localized in the resonant stable islands (in  $\mathcal{I}_0$  but also in  $\mathcal{I}_{\pm}$ ). The number of these states is semiclassically given by the volume of these islands divided by  $2\pi\hbar_{\text{eff}}$ . Far away from quasi-degeneracies, these states are at any time centered on the stable periodic orbit: it can be explained within a semiclassical approach and can be observed in figure 5-c for a state localized in  $\mathcal{I}_0$  and in figures 6-d,e for states in  $\mathcal{I}_-, \mathcal{I}_+$  respectively. Their average velocity as well as their Husimi functions depend exponentially weakly on the Bloch parameter  $k$ .

The last class of states which can be encountered corresponds to chaotic ones, that is to say states whose Husimi functions are negligible on a typical distance of  $\sqrt{\hbar_{\text{eff}}}$  out of the chaotic seas (*cf.* figure 5-a). Unlike the previous ones, their Husimi functions are very sensitive to any variation of  $k$  since they are delocalised in the whole chaotic sea which spreads over all elementary cells. The large classical distribution of possible velocities is to be linked to the very fluctuating slopes of the quasi-energies as  $k$  is varied.

#### D. Tunnelling states

Although the system as a whole is of course time-reversal invariant, this is no longer true for its restriction at a fixed value  $k$  of the Bloch vector. Indeed, the operator  $\tilde{K}$  is not time-reversal invariant, because of the crossed term  $k\hat{p}$ . In other words, the time-reversed partner of a state with Bloch vector  $k$  is a state with Bloch vector  $-k$ . It is only at the special value  $k = 0$  (and also  $k = 1/2$  since  $k$  is defined modulo 1) that  $\tilde{K}$  is invariant under time reversal symmetry. Therefore it corresponds to the typical situation of tunnelling between  $\mathcal{I}_+$  and  $\mathcal{I}_-$ . Every island state localised about  $|p| = 1$  is quasi-degenerate with another one. These doublets represent a symmetric and an antisymmetric combination of states localised in one island only (*cf.* figure 6-f). The energy splitting  $\Delta\epsilon_n$  of these states for  $k = 0$  is precisely the signature of tunnelling: it is  $\pi\hbar_{\text{eff}}$  divided by the typical time an atom takes to jump from one island to its time-reversed image, *i.e.* to reverse the sign of its velocity.

### V. CHAOS ASSISTED TUNNELLING

#### A. Large fluctuations

After having selected the two quasi-energy bands corresponding to the two states which are localized the more deeply inside the islands  $\mathcal{I}_{\pm}$ , we are able to plot the splitting as a function of  $\hbar_{\text{eff}}$ . The great advantage of studying fluctuations when the effective Planck constant is varied is that it does not affect the classical dynamics. The behavior of the splitting is very different whether chaos is present at the  $\hbar_{\text{eff}}$  scale or not. In the chaotic regime (*cf.* figure 7 and 8), that is when  $\hbar_{\text{eff}}$  varies in a range where chaotic seas can be resolved, the splittings vary rapidly versus the change of any parameter, in our case  $\hbar_{\text{eff}}$ . Moreover, the variations of the splittings, despite being perfectly deterministic, are apparently erratic – without any regular structure – and cover several orders of magnitude. They show that direct coupling to the chaotic sea is the key mechanism for their understanding and are a signature of chaos assisted tunnelling [35,36]. In fact these huge fluctuations are reminiscent of the universal conductance fluctuations

---

and define for instance

$$\psi_{n,k}^H(p, q, \tau) \stackrel{\text{def}}{=} N |\langle z, k | \psi_{n,k}(\tau) \rangle|^2 \quad (9)$$

observed in mesoscopic systems [37,38] since tunnelling is nothing else than wave transport from one stability island to the other. In contrast, in the regular regime where chaotic seas are smaller than  $\hbar_{\text{eff}}$ , the splittings are expected to vary smoothly [6].

In figure 7, we show the splittings of the pair of states localized at the center of the resonance islands  $\mathcal{I}_{\pm}$ , as a function of  $\hbar_{\text{eff}}$ . They display huge fluctuations over about 4 orders of magnitude while the general trend is a decrease as  $\hbar_{\text{eff}} \rightarrow 0$ . Similarly, when plotted as a function of  $\gamma$ , see figure 8, they also display large fluctuations. The general trend is here a fast increase of the typical splitting with  $\gamma$ ; this is associated with the shrinking of the regular island when  $\gamma$  increases which results in an increasingly large tunnelling probability. The overlaps of the regular states (still supported by the islands) with the chaotic states increases. Therefore the coupling between the two components of the tunnelling doublets which involves the chaotic states increases as well.

In order to understand both the general trend and the origin of the fluctuations, two points of view can be used: a quantum point of view and a semiclassical one.

## B. Semiclassical interpretation

If the chaotic sea is large, it is rather intuitive that it can be easier to first tunnel from the center of the regular island to the chaotic sea, then propagate freely in the chaotic sea to the vicinity of the symmetric island and finally tunnel to the center of the symmetric island than directly tunnelling between the two islands. The crucial point is that because the chaotic component is explored rapidly and densely, it does not cost anything to cross the chaotic sea. Tunnelling trajectories can be viewed as complex trajectories (i.e. with complex position and momentum) which are real at both the starting (in the initial island) and ending (in the symmetric island) points. The tunnelling amplitude associated with a single tunnelling orbit is essentially  $\exp(-\text{Im}(S)/\hbar_{\text{eff}})$  where  $S$  is the complex action of the tunnelling orbit. In a usual 1-dimensional system (like a double-well), there is only one such trajectory at each energy and the tunnelling rate thus displays the well-known exponential decrease. In a chaotic system, it may happen that there is a whole set of tunnelling trajectories whose imaginary parts of the action are essentially identical. In such conditions, the actual tunnelling amplitude is the sum of all individual amplitudes (each taken with its proper phase) which results in a very complicated quantity which fluctuates when parameters are changed. In some sense, this is analogous to the speckle pattern obtained when plenty of optical rays with various geometries are randomly interfering. This is the very origin of the (deterministic) fluctuations of the tunnelling rates and consequently of the energy splittings. The general trend (exponential decrease) is related to the typical imaginary part of the action of the tunnelling trajectories.

## C. Quantum point of view

A complementary quantum point of view is possible. One can divide the eigenstates of the system in two subsets: the “regular” states localized in the resonance islands and the “chaotic” states localized in the chaotic sea. The two sets are only weakly coupled by tunnelling. Because there are two symmetric islands, the regular states are essentially doubly degenerate (neglecting *direct* tunnelling). The chaotic sea also has the two-fold symmetry and states can be classified as even or odd. The two series of odd and even states are ignoring each other. Hence, when by accident, an even chaotic state is almost degenerate with an even regular state, they repel each other: at the same time, there is usually no odd chaotic state with the same energy. Thus, the odd regular state is not significantly repelled. Hence, the splitting appears because of different shifts of the even and odd regular states. Close to any avoided crossing between either the odd or the even regular state and a corresponding chaotic state, a large splitting is obtained. On the contrary, far from any avoided crossing, the splitting is small. Hence, the fluctuations are just associated with the existence of a large number of successive avoided crossings. The typical size of these fluctuations is related to the typical size of the avoided crossings while the typical parameter range of these fluctuations is the distance (in parameter space) between two consecutive avoided crossings. A model implementing this idea (each regular state is independently and randomly coupled to the chaotic states of the same symmetry) has been proposed in [39] and further used in [40]. In this model, the chaotic states are modeled by a Hamiltonian belonging to the Gaussian Orthogonal Ensemble of random matrices while the coupling between the regular state and the chaotic state is also taken as a random Gaussian variable. With these assumptions, the splitting distribution can be calculated. Let us denote by  $\Delta$  the mean level spacing between chaotic states and by  $\sigma$  the typical strength of the coupling between the regular states and the chaotic sea. Only if  $\sigma \ll \Delta$  is the regular state weakly coupled to the continuum (if this inequality is violated, the regular state is completely diluted in the chaotic sea by the strength of the coupling). We



thus assume the inequality to be valid. Then, the distribution of splittings  $\Delta\epsilon$  is given by:

$$\begin{cases} P(\Delta\epsilon) = \frac{1}{\pi} \frac{s}{s^2 + \Delta\epsilon^2} & \text{for } |\Delta\epsilon| < \sigma \\ P(\Delta\epsilon) \simeq 0 & \text{for } |\Delta\epsilon| > \sigma \end{cases} \quad (11)$$

where

$$s = \frac{\sqrt{2}\pi\sigma^2}{\Delta} \quad (12)$$

The interpretation is rather simple. The maximum splitting is observed exactly at the avoided crossing where the levels are shifted by  $\pm\sigma/2$  on both sides of their unperturbed positions. Hence, the splitting cannot be larger than about  $\sigma$ . In fact, there is an exponentially decreasing tail in the distribution  $P(\Delta\epsilon)$  (associated with the Gaussian fluctuations of  $\sigma$ ) which we do not detail here because it is not relevant in our present case.  $s$  is the typical splitting one expects to observe: it corresponds to the shift typically due to the closest chaotic state. The full distribution is a (truncated) Cauchy distribution: it is obtained as the overall effect of all chaotic states lying above or below in energy. Note that, in the absence of the truncation of the Cauchy distribution, the average splitting is not defined because the corresponding integral diverges. Hence, it is better to discuss the typical splitting  $s$  rather than the average splitting. It is the slow decrease of the Cauchy distribution for large splitting which is responsible for the huge fluctuations in the splittings, which can be as large as  $\sigma \gg s$ . This is reminiscent of random processes such as Lévy flights where rare events are dominant [41].

In fig. 9, we show the statistical distribution of splittings that we obtain numerically in the chaotic regime (normalized to the typical splitting in order to work with  $s = 1$ ). The distribution is shown on a double logarithmic scale and compared with the Cauchy distribution. One can clearly see two regimes: for small  $|\Delta\epsilon|$ ,  $P(|\Delta\epsilon|)$  is almost constant and decreases with a slope -2 for large  $|\Delta\epsilon|$ . The agreement with the Cauchy distribution is very good, which proves that the model catches the essential part of the physics in this system.

The typical splitting  $s$  is proportional to the square of the tunnelling matrix element from the initial state to the chaotic sea. Hence, it is expected to decrease roughly like  $\exp(-2\text{Im}(S)/\hbar_{\text{eff}})$  where  $S$  is the complex action of tunnelling orbits (the mean level spacing scales as a power of  $\hbar_{\text{eff}}$  and is thus a correction to the main exponential decrease). This is roughly what is observed in fig. 7. Note however that there is a plateau in the range  $15 \leq \hbar_{\text{eff}}^{-1} \leq 30$ . A similar observation has been done in [42, fig. 3]. Although this is not a crucial problem (the statistics of the splitting distribution is not affected), a detailed explanation of this behaviour is still lacking, see however [42]. Finally, it should be interesting to calculate explicitly some of the complex tunnelling orbits in our specific system in order to compare the imaginary part of their actions with the slope in fig. 7. This work is currently under progress.

## VI. EXPERIMENTAL SIGNAL

As it can be seen in figure 5, the splittings we want to measure correspond to very tiny scales among the other structures in the band spectrum. For say  $\hbar_{\text{eff}} \simeq 0.1$ , the tunnelling times are about  $\hbar_{\text{eff}}/\Delta\epsilon \sim 10^3$  times the typical period ( $T \sim \text{few } \mu\text{s}$ ). The observation of atoms having reversed their velocity is therefore still possible since during 1 ms spontaneous emission has not begun to spoil our dynamical model. Nevertheless, measuring tiny splittings which are hidden so deeply in the spectrum is far from being straightforward. Several steps are needed: preparation of the initial state, the experiment itself (where chaos assisted tunnelling takes place) and the analysis of the final state. During the first step, one must prepare a state localized inside one resonance island, i.e. localized both in position and momentum spaces. The idea is to use an adiabatic transfer from an initial state extended in position space by slowly branching the effective potential. Although the second step looks trivial (one just has to wait), the dispersion in the vector angle  $k$  makes things much more difficult as only the  $k = 0$  states are related by time-reversal symmetry (see section IV D) and thus tunnel relatively fast. It is however possible to overcome this difficulty as explained below. Finally, the detection should be rather easy, using velocity dependent Raman transitions. We now explain in detail how the various steps can be worked out.

### A. Adiabatic preparation of the atoms in one lateral stable island

The first step consists in preparing an initial cloud of cold Rubidium atoms in order to have it located in one of the stable island, say  $\mathcal{I}_+$ , only. Using a standard magneto-optical trap, one can obtain a more or less thermal distribution of atoms with velocity of the order of few times the recoil velocity  $v_{\text{rec}} = \hbar k_L/M = 6 \text{ mm/s}$ . However – as shown below

– this is probably too much for a good measurement of the tunnelling splitting. Additional techniques (side-band cooling [43], Raman cooling [44,45]) make it possible to obtain a sub-recoil velocity distribution, i.e. atoms with an average momentum  $p_0$  and a thermal dispersion  $\Delta p_x = M\Delta v = M\alpha v_{\text{rec}}$  with  $\alpha$  significantly smaller than 1. We chose the initial momentum to be  $M\delta\omega/2k_L$  so that, on average, the atoms exactly follow one of the sliding standing wave created by a pair  $\omega_{\pm}$  of laser beams.

The next step is to slowly (i.e. adiabatically) switch on the standing waves. During this phase, the spatial periodicity is preserved, and the Bloch vector  $k$  is thus a conserved quantity. Initially, the momentum  $p_x$  is nothing but the Bloch vector (modulo a integer multiple of the recoil momentum). Thus, by preparing a sub-recoil initial state, one populates only a small range of  $k$  values and, for each  $k$  value populated, a single state (momentum eigenstate). Otherwise stated, the initial momentum distribution has become a statistical mixture of Bloch states with  $\Delta k = \alpha/2$  in a single energy band. More generally, if the initial momentum distribution is not a sub-recoil one, but has a width equal to  $\alpha$  recoil momenta (with  $\alpha > 1$ ), about  $\alpha$  bands will be populated.

Switching on the standing waves increases the optical potential  $V_0$  and therefore  $\gamma$  from zero and enlarges the resonance islands. In the sliding frame moving with velocity  $p_0/M = \delta\omega/2k_L$ , the atoms feel a pendulum like potential  $-\frac{1}{2}\gamma \cos q$  (in scaled coordinates) in addition to some rapidly time varying terms. Consequently, they will adiabatically localize in the potential minima, that is at the center of the resonance island. Increasing  $\gamma$  localizes successively an increasing number of states in  $\mathcal{I}_+$ . The switching time must be sufficiently long as compared to the beating period (in this case the discarded terms are still rapidly oscillating) but also to the inverse of the minimum energy gap (of the order of  $\hbar_{\text{eff}}^{-1}$  if  $\Delta k$  is sufficiently narrow). In order to trap all the initially populated states,  $\gamma$  has to be sufficiently large. For a given Bloch angle, we want to localize the  $\alpha$  first states. The quantum energies of a pendulum are given by the eigenvalues of the Mathieu equation [46, chap. 20] (see figures 10 and 11). For a pendulum whose hamiltonian is

$$H_{\text{pend}} = \frac{p^2}{2} - \frac{\gamma}{2} \cos q, \quad (13)$$

the phase space volume enclosed by the separatrix is given  $16\sqrt{\gamma/2}$ . Semiclassically, it corresponds to  $16\sqrt{\gamma/2}/(2\pi\hbar_{\text{eff}})$  states. This number will be of the order of  $\alpha$  when  $\gamma$  reaches the value:

$$\gamma_{\text{adiab}} \simeq \frac{(\alpha\pi\hbar_{\text{eff}})^2}{128}. \quad (14)$$

Figures 10 and 11 show the exact energy levels of the system together with the ones using the pendulum approximation and the Mathieu equation, as well as plots of selected Husimi representations for few eigenstates. This allows to check that :

- The pendulum approximation works well in the regime of interest, say up to  $\gamma = 0.1$ .
- The semiclassical estimate of the number of trapped states is sufficiently accurate for our purpose.
- The Husimi representations of the trapped states are well localized: especially, the states in figure 11 have two well separated components in the  $\mathcal{I}_+$  and  $\mathcal{I}_-$  islands, meaning that we are in a real case of tunnelling.
- During the initial increase of  $\gamma$ , the “ground” state is well isolated (in energy) from the other ones, which means that an adiabatic preparation is possible.

Nevertheless, for this adiabatic preparation to be valid, we must make sure that  $\gamma$  has not reached a range where chaos have non negligible effects on quantum properties. Physically, we want that chaotic layers at  $\gamma = \gamma_{\text{adiab}}$  have a small volume compared to the Planck constant. From figure 10, we can obtain the upper bound limit of  $\gamma$  by estimating when the (small) avoided crossings become too large to be passed diabatically. For  $1/50 < \hbar_{\text{eff}} < 1/5$ , we observe that chaos have no influence for  $\gamma < \gamma_{\text{chaos}} \simeq 0.04$ .

The adiabatic preparation of all the atoms in one stable island will be achieved if  $\gamma_{\text{adiab}} < \gamma_{\text{chaos}}$  that is if the atoms are cold enough to have

$$\alpha < \frac{8\sqrt{2\gamma_{\text{chaos}}}}{\pi\hbar_{\text{eff}}} \simeq \frac{0.7}{\hbar_{\text{eff}}}. \quad (15)$$

In every situation considered in the following, we will have to check that this condition is fulfilled. Next we have to reach the desired value for  $\gamma$  ( $\simeq 0.18$ ) in the chaotic regime while preserving the state in the island. This will be achieved if  $\gamma$  is increased sufficiently fast so that all encountered avoided crossings with chaotic states are passed diabatically.

Hence the whole preparation of the initial atomic state proceeds by two steps: a first adiabatic increase of  $\gamma$  at the very beginning to significantly populate regular states in one island followed by a diabatic increase of  $\gamma$  to preserve them in the chaotic regime.

## B. How to force tunnelling ?

As discussed in section IV D, the tunnelling splitting is small only for Bloch vector  $k = 0$ . As it is not presently possible to prepare only this value of  $k$  in a real experiment, it seems at first sight that only a small fraction of atoms (close to  $k = 0$ ) may effectively tunnel, hence considerably reducing the signal to noise ratio. A solution is to force all atoms to go through the  $k \approx 0$  region. The simplest idea is to impose a slow increase of the  $k$  value, by adding a constant external force  $F$  from outside. Then, the full Hamiltonian which governs the dynamics is:

$$H'(p, q, \tau) = H(p, q, \tau) - qF . \quad (16)$$

The potential  $V$  induces a dynamical drift in the Bloch angle:

$$\frac{d}{d\tau}k(\tau) = \frac{1}{\hbar_{\text{eff}}}F . \quad (17)$$

It is shown in appendix C that this relation, which is well-known in the time independent case (see for instance [47, chap.6]), remains valid when  $H$  is periodic in time.

A convenient way of realizing experimentally such a constant force is to chirp the laser frequencies, that is make all the frequencies drift linearly in time. In an accelerated frame, the laser frequencies appear as constant, and we are back to our model. However, in this non inertial frame, the constant acceleration is translated in a constant force, hence the system is governed by equation (16). This method has been used with cold atoms, see [19].

The global result is a slow drift of the  $k$  distribution. This makes that the various  $k$  classes successively come close to  $k = 0$  and are thus able to tunnel. Whether the atom will effectively tunnel or not depends on the time scale on which  $k$  changes. If  $k$  varies rapidly, the avoided crossing at  $k = 0$  is crossed diabatically, i.e. the velocity distribution will not be modified. If  $k$  varies slowly, it is crossed adiabatically (rapid adiabatic passage). The Landau-Zener formula [48] yields for the typical time scale for the crossover between diabatic and adiabatic crossing.

Figures 12 and 13 illustrate, for  $\hbar_{\text{eff}} = 0.2037$  the drift of atoms initially localized in  $\mathcal{I}_+$  (one energy band) whose distribution in  $k$  covers 1/10 of the Brillouin zone from  $k \simeq -1/10$  to  $k \simeq 0$  (sub-recoil initial velocity distribution with width of the order of  $v_{\text{rec}}/5$ ) Let us have the atoms evolving under the force  $F$  in order to get a global translation of 1/10 in  $k$ . After a sliding across the splitting at  $k = 0$ , if the force  $F$  is weak to follow the energy level adiabatically, the average momentum of the atoms has reversed its sign as can be seen on figure 13. Measuring the critical value of  $F$  for this Landau-Zener like transition to occur furnishes a mean to measure the splitting.

Another possibility would be to modulate the external force (and thus the  $k$  values) periodically in time in order to induce a resonant transfer between  $\mathcal{I}_+$  and  $\mathcal{I}_-$ .

In any case, the method may work only if no other avoided crossing come into play. Numerical investigations show that there are mainly tiny avoided crossings along the energy curve of interest. However, as a general rule, there are usually few avoided crossings with similar or larger size than the avoided crossing of interest. If such an avoided crossing is also passed adiabatically, it will of course spoil the momentum distribution. Hence, it is crucial for the initial  $k$  distribution to be sufficiently narrow to avoid this problem. Hence, a sub-recoil velocity distribution seems necessary.

## C. Detection

After the atoms have interacted with the modulated waves, one can switch off the lasers either abruptly or adiabatically (in which case the atoms adiabatically leave the resonance island). In both cases, the atoms which have tunneled from  $\mathcal{I}_+$  to  $\mathcal{I}_-$  will end with a momentum close to  $-p_0$ . A standard time of flight technique should be enough to detect them. A more sophisticated technique, for example based on velocity sensitive Raman transitions [49,43] could also be used with a subrecoil resolution if needed [19].

## VII. CONCLUSION

In this paper we have proposed a simple and accessible experimental configuration in which the observation of chaos assisted tunnelling should be feasible. It consists in atoms propagating in the light field of two far-detuned monochromatic standing waves with slightly different frequencies. Observing the tunnelling effect however requires sub-recoil cooling techniques to conveniently prepare the atomic sample together with a well-controlled experimental

procedure (adiabatic preparation of the atomic state in one stable island followed by a drift of the Bloch vector). As the tunnelling period fluctuates over several decades when the potential strength varies (see fig.8), observing these fluctuations requires a stabilization of the laser intensity at the level of a few percent.

## ACKNOWLEDGMENTS

Ch. M., R. K. and A. M. would like to thank the Laboratoire Kastler Brossel for kind hospitality. CPU time on computers has been provided by IDRIS. Laboratoire Kastler Brossel de l'Université Pierre et Marie Curie et de l'École Normale Supérieure is UMR 8552 du CNRS.

## APPENDIX A: DERIVATION OF THE EFFECTIVE HAMILTONIAN

To derive the effective Hamiltonian (2), we basically proceed in three steps [50] :

- We first assume that any dissipation process can be safely ignored. Indeed for tunnelling to be observable, phase coherence of the atomic wave-function must be preserved during all the process. In our case, this means that spontaneous emission must be negligible. It can be shown [51] that increasing the laser detuning considerably decreases phase coherence loss. Hence the evolution will be essentially Hamiltonian provided each laser beam is sufficiently far-detuned from the atomic resonance :

$$|\delta_{\pm}| = |\omega_{\pm} - \omega_{\text{at}}| \gg \Gamma \quad (\text{A1})$$

When this holds, the total Hamiltonian operator for this two-level system is the sum of three terms: the kinetic energy operator describing the center-of-mass motion of atoms of mass  $M$  the energy operator for the internal degrees of freedom and the coupling between internal and external degrees of freedom. In the dipolar approximation, the interaction is just  $dE(x, t)$  and does not depend on  $y$  and  $z$ . The dynamics along  $y$  and  $z$  is just trivially described by free motion and can be easily eliminated since the total quantum state factorizes as a plane wave in  $y$  and  $z$ . One is then left with the dynamics along  $x$  which is described by the hamiltonian :

$$H_{\text{at}} = \frac{p_x^2}{2M} (|e\rangle\langle e| + |g\rangle\langle g|) + \hbar\omega_{\text{at}}|e\rangle\langle e| - dE(x, t)(|e\rangle\langle g| + |g\rangle\langle e|) \quad (\text{A2})$$

where  $p_x$  is the atomic momentum along  $x$ .  $|g\rangle$  and  $|e\rangle$  are the ground-state and excited-state and  $d$  is the atomic dipole strength connecting them.

- Second, we expand the total atomic state as:

$$|\Psi\rangle = \psi_g(x, t)|g\rangle + \psi_e(x, t) \exp(-i\omega_L t)|e\rangle \quad (\text{A3})$$

and we drop high frequency (optical) anti-resonant terms as far the amplitudes change slowly during an optical period. This is known as the rotating wave approximation [52] and features the averaging procedure to eliminate fast variables in classical perturbation theory [25]. This yields the coupled amplitude equations:

$$i\hbar\partial_t\psi_g = -\frac{\hbar^2}{2M}\partial_{xx}^2\psi_g - \frac{\hbar\Omega(x, t)}{2}\psi_e ; \quad (\text{A4a})$$

$$i\hbar\partial_t\psi_e = -\frac{\hbar^2}{2M}\partial_{xx}^2\psi_e - \hbar\delta_L\psi_e - \frac{\hbar\Omega^*(x, t)}{2}\psi_g . \quad (\text{A4b})$$

In these equations  $\delta_L = \omega_L - \omega_{\text{at}}$  is the mean laser detuning, the star denotes complex conjugation and  $\Omega(x, t)$  reads:

$$\Omega(x, t) = [\Omega_+ \exp(-i\delta\omega t/2) + \Omega_- \exp(i\delta\omega t/2)] \cos(k_L x) \quad (\text{A5})$$

where  $\Omega_{\pm} = dE_{\pm}/\hbar$  are the Rabi frequencies of each standing wave.

- As a final step, we assume now that atoms initially prepared in their ground-state mostly evolve in their ground-state. This means that the whole atomic dynamics is solely determined by the ground-state amplitude  $\psi_g$ . For this to hold, adiabatic elimination of the excited-state amplitude [51] must be justified. If the spatial partial derivatives were absent, equations (A4) would just describe the Rabi oscillation phenomenon. It is then known that far off resonance, i.e. when the frequency separation of the states is much larger than any other frequencies, the Rabi oscillation is very small in amplitude. A sufficient condition is :

$$|\delta_L| \gg \Omega_{\pm}, \delta\omega \quad (\text{A6})$$

If in addition we assume that the excited-state kinetic energy is very small (which will be easily achieved with cold atoms):

$$|\delta_L| \gg \left\langle \psi_e \left| \frac{p_x^2}{2M} \right| \psi_e \right\rangle \quad (\text{A7})$$

then adiabatic elimination of the excited-state amplitude just amount to neglect the spatial and temporal derivatives of  $\psi_e$  in equation (A4b) which is then solved as  $\psi_e \simeq -(\Omega^*/2\delta_L)\psi_g \ll \psi_g$ . It is then easy to see that the ground-state amplitude  $\psi_g$  obeys an effective Schrödinger equation with Hamiltonian:

$$H = \frac{p_x^2}{2M} + \frac{\hbar|\Omega(x, t)|^2}{4\delta_L}. \quad (\text{A8})$$

Eventually, up to an irrelevant purely time-dependent term, we get

$$H = \frac{p_x^2}{2M} - V_0 \cos(2k_L x) [\theta + \cos(\delta\omega t)] \quad (\text{A9})$$

where  $V_0 \stackrel{\text{def}}{=} -\hbar\Omega_+\Omega_-/8\delta_L$  and  $\theta \stackrel{\text{def}}{=} (\Omega_+/2\Omega_-) + (\Omega_-/2\Omega_+)$ .

## APPENDIX B: FLOQUET-BLOCH FORMALISM

In this appendix, we briefly recall the Floquet-Bloch formalism which is used for a quantum problem whose Hamiltonian  $H$  is periodic both in space and in time. We will denote  $T$  and  $Q$  the temporal and spatial periods respectively.

Let us first consider the time periodicity. We define [29,31,53]

$$K(\hat{p}, \hat{q}, \tau) \stackrel{\text{def}}{=} -i\hbar \frac{d}{d\tau} + H(\hat{p}, \hat{q}, \tau) \quad (\text{B1})$$

where  $\hat{p}$  and  $\hat{q}$  stand for canonical Hermitian operators whose commutator is  $[\hat{p}, \hat{q}] = -i\hbar$ .

If  $U(\tau', \tau)$  denotes the unitary evolution operator from  $\tau$  to  $\tau'$  associated with Hamiltonian  $H$ , the periodicity of the dynamics implies that  $U(\tau + T, T) = U(\tau, 0)$  and

$$U(\tau + T, \tau) = U(\tau + T, T) U(T, 0) U(0, \tau) = [U(0, \tau)]^{-1} U(T, 0) U(0, \tau). \quad (\text{B2})$$

This shows that  $U(\tau + T, \tau)$  and  $U(T, 0)$  differ by a unitary transformation and hence have the same spectrum (but of course different eigenvectors), independent of  $\tau$ . The eigenvalues of  $U(\tau + T, \tau)$  have unit modulus and can be written as  $e^{-i\epsilon_n T/\hbar}$  where  $\epsilon_n$  is the so-called quasi-energy defined modulo  $2\pi\hbar/T$ . If  $|\psi_n(\tau)\rangle$  denotes the corresponding eigenvector, we can define the Floquet state:

$$|\chi_n(\tau)\rangle \stackrel{\text{def}}{=} e^{i\epsilon_n \tau/\hbar} |\psi_n(\tau)\rangle \quad (\text{B3})$$

which is by construction periodic with period  $T$ .

Inserting the definition of the Floquet state in the time-dependent Schrödinger equation, we immediately obtain:

$$K(\hat{p}, \hat{q}, \tau) |\chi_n(\tau)\rangle = \epsilon_n |\chi_n(\tau)\rangle. \quad (\text{B4})$$

which means that the quasi-energy spectrum is obtained by diagonalizing the Floquet Hamiltonian in the space of time-periodic functions.

The second step consists in making use of the invariance of  $H$  under spatial translations with period  $Q$ . The unitary translation operator  $\hat{T}_Q \stackrel{\text{def}}{=} e^{-i\hat{p}Q/\hbar}$  commutes with  $K$ . We can then use the spatial counterpart of the Floquet theorem, namely the Bloch theorem [28], and label the eigenstates of  $K$  with the Bloch number  $k \in [-\pi/Q, \pi/Q[$  (the first Brillouin zone), which means diagonalising  $K$  in each subspace with fixed  $k$ . If one defines the Floquet-Bloch states as:

$$|u_{n,k}(\tau)\rangle = e^{-ik\hat{q}}|\chi_{n,k}(\tau)\rangle = e^{i\epsilon_n(k)\tau/\hbar}e^{-ik\hat{q}}|\psi_{n,k}(\tau)\rangle, \quad (\text{B5})$$

where  $\{|\psi_{n,k}(\tau)\rangle\}$  forms a complete orthogonal eigenbasis, it is easy to show that they can be obtained by diagonalizing the Floquet-Bloch Hamiltonian:

$$\tilde{K}(\hat{p}, \hat{q}, \tau, k) = K(\hat{p} + \hbar k, \hat{q}, \tau) \quad (\text{B6})$$

on the subspace of time and space periodic functions. In our specific case, the Floquet-Bloch Hamiltonian reads:

$$\tilde{K}(\hat{p}, \hat{q}, \tau, k) = \frac{(\hat{p} + \hbar k)^2}{2} - \gamma (\theta + \cos \tau) \cos \hat{q} - i\hbar \frac{d}{d\tau}. \quad (\text{B7})$$

The spatial periodicity of the Floquet-Bloch states leads to a discrete set of dispersion relations  $\epsilon_n(k)$ . For fixed  $n$ , the set of all quasi-energies  $\epsilon_n(k)$  for  $k$  in the first Brillouin zone  $[-\pi/Q, \pi/Q[$  is called the  $n$ th band of the system.

Let us now obtain the velocity theorem (10). Using the above relations, we have  $\langle \psi_{\epsilon,k}(\tau) | \hat{p} | \psi_{\epsilon,k}(\tau) \rangle = \langle u_{\epsilon,k}(\tau) | (\hat{p} + \hbar k) | u_{\epsilon,k}(\tau) \rangle = \langle u_{\epsilon,k}(\tau) | (\hbar^{-1} \partial \tilde{K} / \partial k) | u_{\epsilon,k}(\tau) \rangle$ . The derivation with respect to  $k$  of the relation  $\langle u_{\epsilon,k}(\tau) | \tilde{K} | u_{\epsilon,k}(\tau) \rangle = \epsilon(k)$  leads to

$$\begin{aligned} & \langle \psi_{\epsilon,k}(\tau) | \hat{p} | \psi_{\epsilon,k}(\tau) \rangle \\ &= \frac{1}{\hbar} \frac{\partial \epsilon}{\partial k} + i\hbar \frac{d}{d\tau} \left( \langle u_{\epsilon,k}(\tau) | \frac{\partial}{\partial k} | u_{\epsilon,k}(\tau) \rangle \right) - \left( \frac{1}{\hbar} \frac{\partial}{\partial k} \langle u_{\epsilon,k}(\tau) | \tilde{K} | u_{\epsilon,k}(\tau) \rangle \right) - \left[ \left( \frac{1}{\hbar} \frac{\partial}{\partial k} \langle u_{\epsilon,k}(\tau) | \tilde{K} | u_{\epsilon,k}(\tau) \rangle \right) \right]^* . \end{aligned} \quad (\text{B8})$$

The two last terms of the the right hand side are opposite since the normalization of the  $u$ 's leads to  $\partial \langle u_{\epsilon,k} | u_{\epsilon,k} \rangle / \partial k = 0$ . Moreover, after time-averaging (B8) over  $T$ , the total  $\tau$ -derivative vanishes since the  $u$ 's are precisely  $T$ -periodic while the time-independent  $k$ -derivative of the quasi-energy remains unchanged. Eventually,

$$\frac{1}{T} \int_0^T \langle \psi_{\epsilon,k}(\tau) | \hat{p} | \psi_{\epsilon,k}(\tau) \rangle d\tau = \frac{1}{\hbar} \frac{\partial \epsilon}{\partial k}. \quad (\text{B9})$$

### APPENDIX C: BLOCH ANGLE DYNAMICS

In this appendix we derive equation (17) which is valid for an arbitrary strength of the constant force  $F$  provided that the potential  $V = -Fq$  remains strictly linear in  $q$ . Let us choose a state  $|\psi(\tau)\rangle$  evolving under  $H' = H + V$  such that it coincides with a Floquet-Bloch state at  $\tau = 0$ :

$$i\hbar_{\text{eff}} \frac{d|\psi(\tau)\rangle}{d\tau} = H'(\hat{p}, \hat{q}, \tau) |\psi(\tau)\rangle \quad (\text{C1})$$

and

$$|\psi(\tau = 0)\rangle = |\psi_{n,k}(\tau = 0)\rangle. \quad (\text{C2})$$

In the interaction picture we have immediately

$$i\hbar_{\text{eff}} \frac{d|\psi^I(\tau)\rangle}{d\tau} = -FU^\dagger(\tau, 0)\hat{q}U(\tau, 0)|\psi^I(\tau)\rangle \quad (\text{C3})$$

where  $|\psi^I(\tau)\rangle \stackrel{\text{def}}{=} U^\dagger(\tau, 0)|\psi(\tau)\rangle$  and where  $U$  denotes the evolution operator under  $H$ . Let  $|\phi(\tau)\rangle$  be the ket defined by

$$|\phi(\tau)\rangle \stackrel{\text{def}}{=} e^{-iF\hat{q}\tau/\hbar_{\text{eff}}}|\psi^I(\tau)\rangle. \quad (\text{C4})$$

It is straightforward to obtain its evolution :

$$i\hbar_{\text{eff}} \frac{d|\phi(\tau)\rangle}{d\tau} = G(\tau) |\phi(\tau)\rangle \quad (\text{C5})$$

where

$$G(\tau) \stackrel{\text{def}}{=} F \left( \hat{q} - e^{-i\tau F \hat{q} / \hbar_{\text{eff}}} U^\dagger(\tau, 0) \hat{q} U(\tau, 0) e^{i\tau F \hat{q} / \hbar_{\text{eff}}} \right). \quad (\text{C6})$$

Since  $U^\dagger(\tau, 0)$  commutes with the translation operator  $\hat{T}_Q$ , it can be checked that  $[G(\tau), \hat{T}_Q] = 0$ . The evolution of  $|\phi(\tau)\rangle$  under  $G$  will therefore preserve its initial quantum number  $k$  :

$$\hat{T}_Q |\phi(\tau)\rangle = e^{-ikQ} |\phi(\tau)\rangle \quad (\text{C7})$$

for all  $\tau$ . Thus, making use of (C3) and (C4), we have

$$\hat{T}_Q |\psi(\tau)\rangle = e^{-i(k + F\tau/\hbar_{\text{eff}})Q} |\psi(\tau)\rangle \quad (\text{C8})$$

which shows that  $|\psi(\tau)\rangle$  is actually a Bloch wave with a Bloch angle given by  $k(\tau) = k(0) + F\tau/\hbar_{\text{eff}}$  even if it spreads among the quasi-energy bands.

- [1] in *Chaos et Physique Quantique — Chaos and Quantum Physics*, Les Houches, école d'été de physique théorique 1989, session LII, edited by M. Giannoni, A. Voros, and J. Zinn-Justin (North-Holland, Amsterdam, 1991).
- [2] E. Heller, Phys. Rev. Lett. **53**, 1515 (1984).
- [3] in *Mesoscopic quantum physics*, Les Houches, école d'été de physique théorique 1994, session LXI, edited by E. Akkermans, G. Montambaux, J. Pichard, and J. Zinn-Justin (North-Holland, Amsterdam, 1995).
- [4] A. Messiah, *Mécanique Quantique (2 vol.)* (Dunod, Paris, 1964), english translation: North-Holland (Amsterdam).
- [5] R. Balian and C. Bloch, Ann. Physics **84**, 559 (1974).
- [6] M. Wilkinson, Physica D **21**, 341 (1986).
- [7] M. Wilkinson and J. H. Hannay, Physica D **27**, 201 (1987).
- [8] W. Lin and L. Ballentine, Phys. Rev. Lett. **65**, 2927 (1990).
- [9] O. Bohigas, D. Boosé, R. Egidio de Carvalho, and V. Marvulle, Nuclear Phys. A **560**, 197 (1993).
- [10] O. Bohigas, S. Tomsovic, and D. Ullmo, Phys. Rep. **223**, 43 (1993).
- [11] S. Tomsovic and D. Ullmo, Phys. Rev. E **50**, 145 (1994).
- [12] S. C. Creagh and N. D. Whelan, Phys. Rev. Lett. **77**, 4975 (1996).
- [13] V. Averbukh, N. Moiseyev, B. Mirbach, and H. J. Korsh, Z. Phys. D **35**, 247 (1995).
- [14] in *Laser and manipulation of atoms and ions*, Enrico Fermi international summer school, Course CXVIII, 9-19 July 1991, edited by E. Arimondo, W. D. Phillips, and F. Strumia (North-Holland, Amsterdam, 1992).
- [15] *Atom Interferometry*, edited by P. R. Berman (Academic Press, New York, 1996).
- [16] M. Weidemüller, A. Hemmerich, A. Görlitz, T. Esslinger, and T. W. Hänsch, Phys. Rev. Lett. **75**, 4583 (1995).
- [17] L. Guidoni, C. Triché, P. Verkerk, and G. Grynberg, Phys. Rev. Lett. **79**, 3363 (1997).
- [18] K. Drese and M. Holthaus, Phys. Rev. Lett. **78**, 2932 (1997).
- [19] M. Ben Dahan, E. Peik, J. Reichel, Y. Castin, and C. Salomon, Phys. Rev. Lett. **76**, 4508 (1996).
- [20] Q. Niu, X.-G. Zhao, G. A. Georgakis, and M. G. Raizen, Phys. Rev. Lett. **76**, 4504 (1996).
- [21] F. L. Moore, J. C. Robinson, C. Bharucha, P. E. Williams, and M. G. Raizen, Phys. Rev. Lett. **73**, 2974 (1994).
- [22] G. Labeyrie, F. de Tomasi, J. Bernard, C. A. Müller, C. Miniatura, and R. Kaiser, Phys. Rev. Lett. **83**, 5266 (1999).
- [23] T. Jonckheere, C. A. Müller, R. Kaiser, C. Miniatura, and D. Delande, Phys. Rev. Lett. **85**, 4269 (2000).
- [24] C. Cohen-Tannoudji, J. Dupont-Roc, and G. Grynberg, *Processus d'interaction entre photons et atomes, Savoirs actuels* (InterEditions/Éditions du CNRS, Paris, 1988), english translation: Wiley and sons (New York).
- [25] A. J. Lichtenberg and M. A. Lieberman, *Regular and Stochastic Motion*, Vol. 38 of *Applied Mathematical Sciences* (Springer-Verlag, New York, 1983).
- [26] B. Chirikov, Phys. Rep. **52**, 263 (1979).
- [27] M. J. Davis and E. J. Heller, J. Phys. Chem. **85**, 307 (1981).
- [28] N. W. Ashcroft and N. D. Mermin, *Solid State Physics* (Saunders College, Philadelphia, 1976).
- [29] G. Floquet, Ann. de l'Éc. Normale, 2<sup>e</sup> Série **12**, 47 (1883), (in french).
- [30] T. M. Cherry, Proc. London Math. Soc. (2nd ser.) **26**, 211 (1927).
- [31] J. H. Shirley, Phys. Rev. **138**, B979 (1965).
- [32] W. H. Louisell, *Quantum statistical properties of radiation* (Wiley, chichester, 1973).
- [33] J. von Neumann and E. Wigner, Phys. Z. **30**, 467 (1929), english translation in [55] pp. 167–172: On the Behavior of the Eigenvalues in Adiabatic Processes.

- [34] P. Leboeuf and A. Voros, in *Quantum chaos — Between order and disorder*, edited by G. Casati and B. Chirikov (Cambridge University Press, Cambridge, 1992), pp. 507–533. See Ref. [54].
- [35] E. M. Zanardi, Gutiérrez, and J. M. Gomez Llorente, *Phys. Rev. E* **5**, 4736 (1995).
- [36] J. Zakrzewski, D. Delande, and A. Buchleitner, *Phys. Rev. E* **57**, 1458 (1998).
- [37] S. Washburg and R. Webb, *Adv. in Phys.* **35**, 375 (1986).
- [38] S. Feng and P. A. Lee, *Science* **251**, 633 (1991).
- [39] F. Leyvraz and D. Ullmo, *J. Phys. A* **29**, 2529 (1996).
- [40] J. Zakrzewski and D. Delande, *Phys. Rev. E* **47**, 1650 (1993).
- [41] J.-P. Bouchaud and A. Georges, *Phys. Rep.* **195**, 127 (1990).
- [42] R. Roncaglia, L. Bonci, F. M. Izrailev, B. J. West, and P. Grigolini, *Phys. Rev. Lett.* **73**, 802 (1994).
- [43] M. Morinaga, I. Bouchoule, J.-C. Karam, and C. Salomon, *Phys. Rev. Lett.* **83**, 4037 (1999).
- [44] M. Kasevich and S. Chu, *Phys. Rev. Lett.* **69**, 1741 (1992).
- [45] J. Reichel, F. Bardou, M. Ben Dahan, E. Peik, S. Rand, C. Salomon, and C. Cohen-Tannoudji, *Phys. Rev. Lett.* **75**, 4575 (1995).
- [46] M. Abramowitz and I. A. Segun, *Handbook of mathematical functions* (Dover publications, New York, 1965).
- [47] J. Callaway, *Quantum Theory of the Solid State* (Academic Press, London and New York, 1974), Vol. B.
- [48] C. Zener, *Proc. Roy. Soc. London Ser. A* **137**, 696 (1932).
- [49] V. Vuletić, C. Chin, A. J. Kerman, and S. Chu, *Phys. Rev. Lett.* **81**, 5768 (1998).
- [50] R. Graham, M. Schlautmann, and P. Zoller, *Phys. Rev. A* (3) **45**, R19 (1992).
- [51] C. Cohen-Tannoudji, in *Systèmes fondamentaux en optique quantique — Fundamental Systems in Quantum Optics*, Les Houches, école d'été de physique théorique 1990, session LIII, edited by J. Dalibard, J.-M. Raimond, and J. Zinn-Justin (North-Holland, Amsterdam, 1990), pp. 1–164.
- [52] A. L. C. and J. Eberly, *Optical Resonance and Two Level Atoms* (Dover, New York, 1987).
- [53] Y. B. Zeldovich, *Soviet Phys. JETP* **24**, 1006 (1967), translated from the original article (1966) in russian.
- [54] *Quantum chaos — Between order and disorder*, edited by G. Casati and B. Chirikov (Cambridge University Press, Cambridge, 1995).
- [55] R. S. Knox and A. Gold, *Symmetry in the solid state, Lecture notes and supplements in physics* (W. A. Benjamin, Inc, New York, 1964).



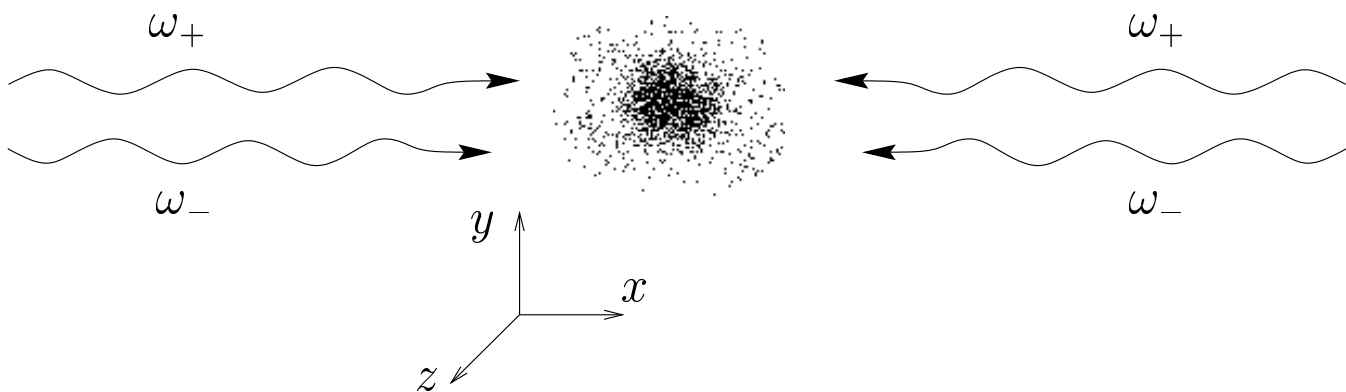


FIG. 1. Experimental configuration under consideration: a cloud of two-level atoms is exposed to two monochromatic standing waves with frequencies  $\omega_{\pm} = \omega_L \pm \delta\omega/2$  ( $\delta\omega \ll \omega_L$ ). All fields are linearly polarised along the same direction and are sufficiently far-detuned from the atomic resonance so that dissipation effects can be ignored.

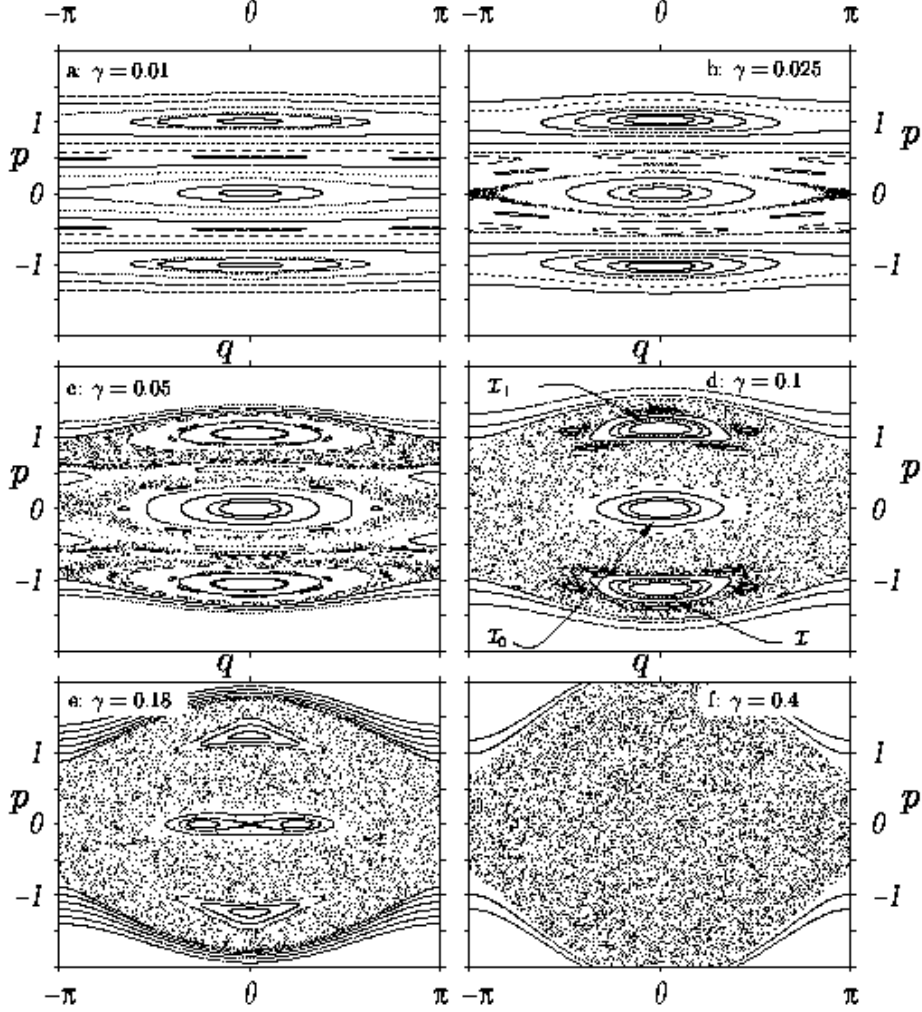
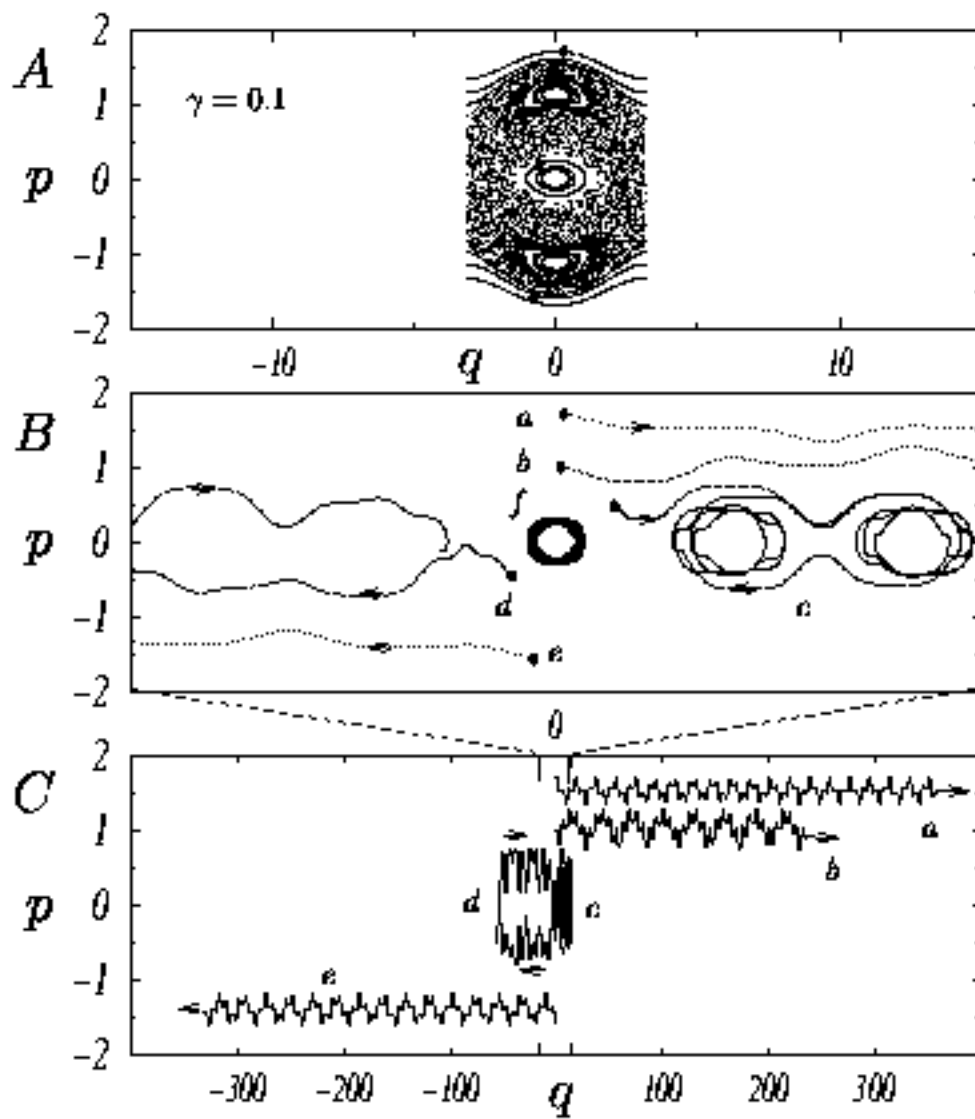
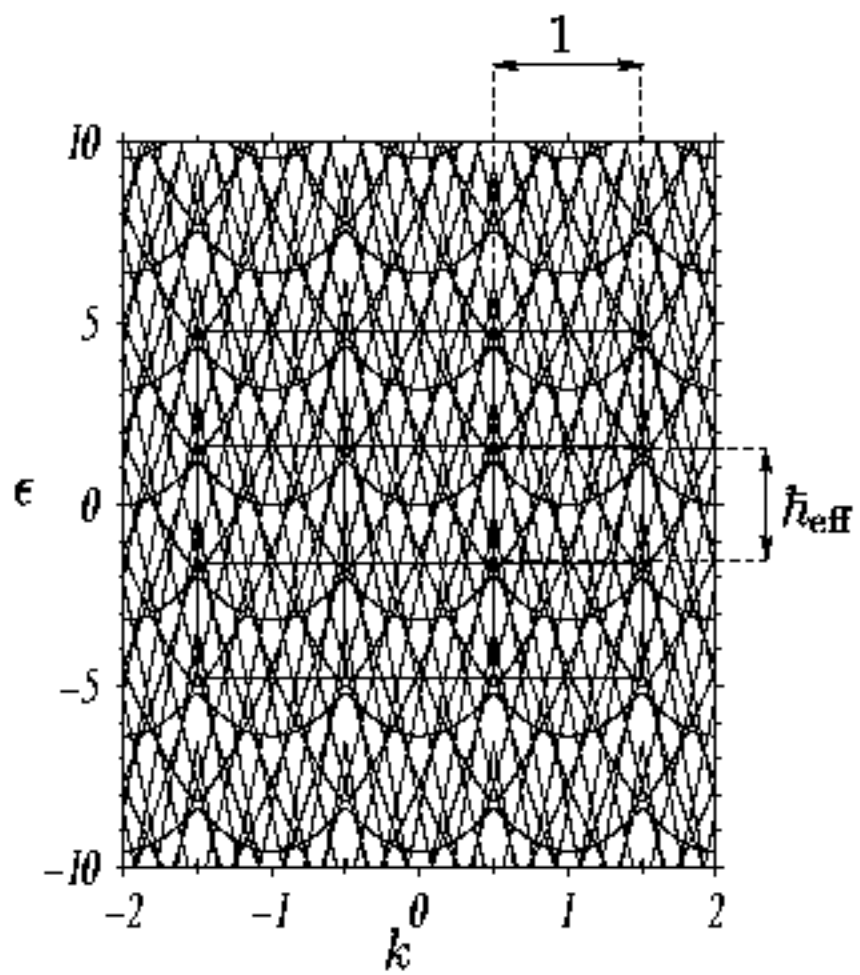
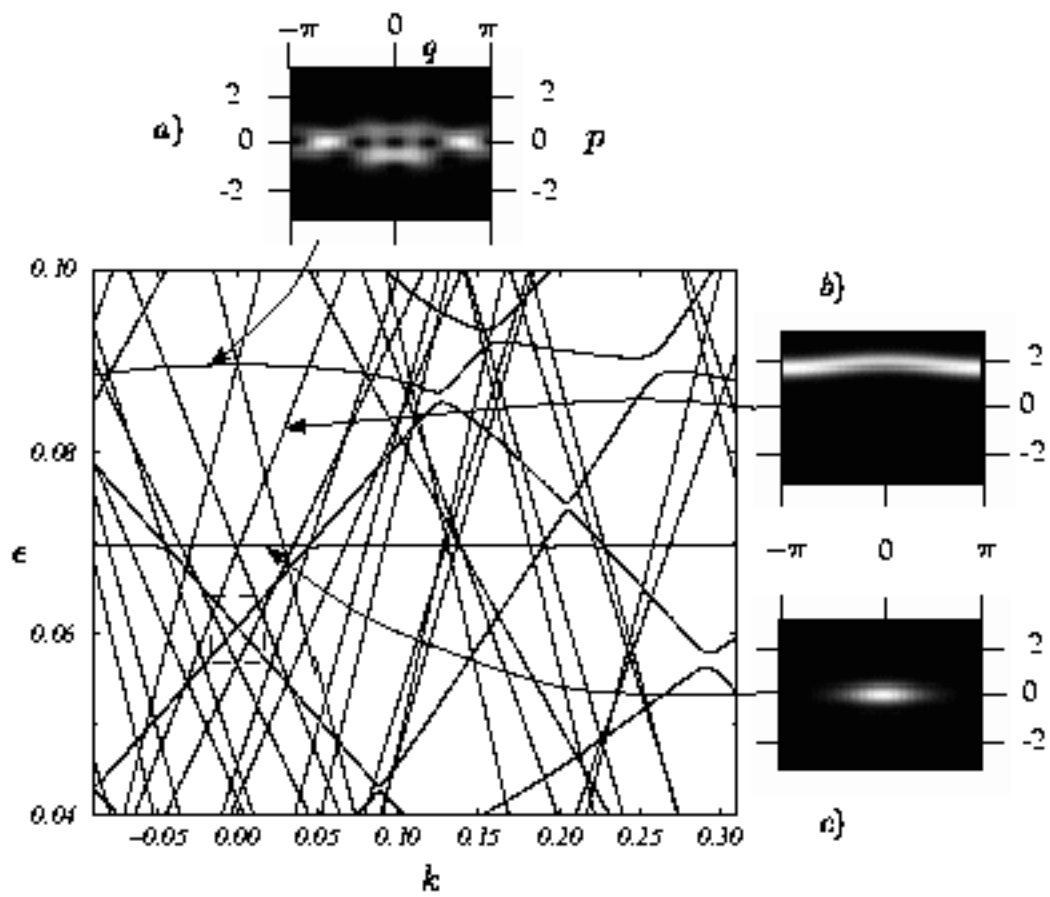


FIG. 2. Stroboscopic plots of trajectories in phase space for different initial conditions at  $\tau = 0$  and different  $\gamma$ 's. The classical dynamics is governed by Hamiltonian (3) with  $\theta = 1$ . At low  $\gamma$  values, resonance islands are visible separated by quasi-free motion. As  $\gamma$  increases, the resonance islands grow and chaos appears close to the separatrices. The situation of interest for chaos assisted tunnelling is when two symmetric islands are separated by a chaotic sea, as  $\mathcal{I}_+$  and  $\mathcal{I}_-$  in (d) and (e).







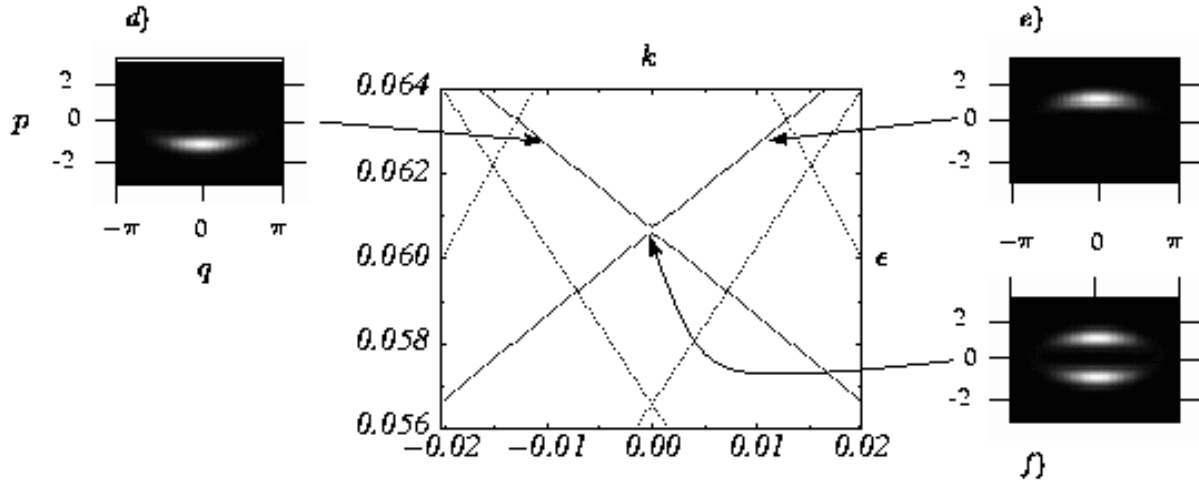


FIG. 6. Quasi-energy bands for  $\gamma = 0.18$  and  $\hbar_{\text{eff}} = 0.2037$  and some Husimi representations of typical states. It is a zoom of the dashed squared zone in figure 5. For  $k \neq 0$ , one can find states, like in  $d$  or  $e$ , whose Husimi function is localised in one stable island  $\mathcal{I}_-$  or  $\mathcal{I}_+$  (compare with figure 2-e). In the frame where the center of the island is fixed, these states correspond to the “ground” states (some excited states may of course exist if  $\hbar_{\text{eff}}$  is small enough as can be seen in figures 12 and 13). For  $k = 0$ , we recover time reversal symmetry through the existence of quasidegenerate doublets of symmetric or antisymmetric combinations. This is the typical tunnelling situation: following adiabatically with  $k$  the state in  $e$  (which has an average velocity about +1), by decreasing  $k$  we get the state in  $d$  which has a reversed velocity. This reversal of the velocity is a classically forbidden process (compare with orbit  $h$  in figure 3).

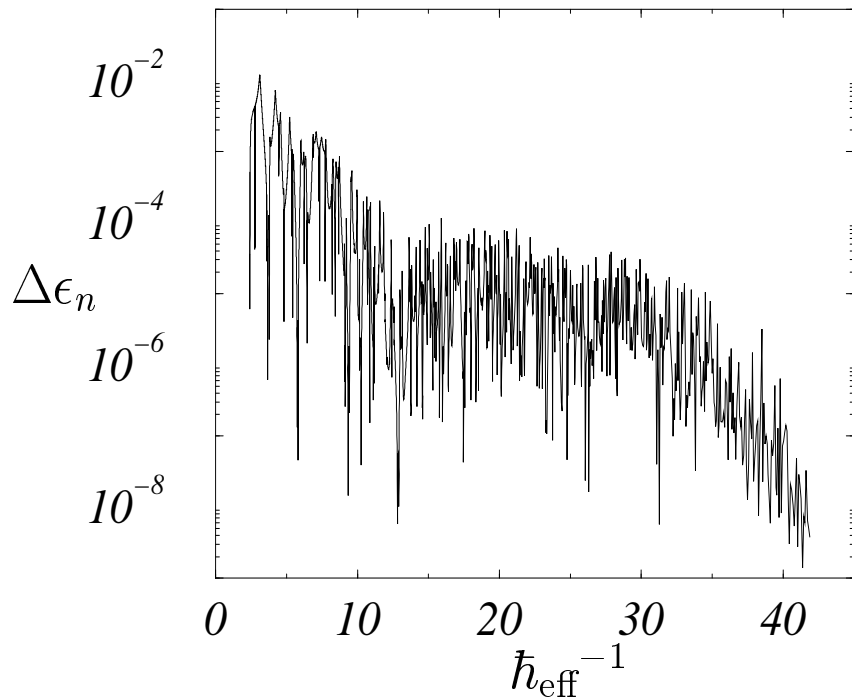


FIG. 7. Fluctuations of the energy splittings  $\Delta\epsilon_n$  between pairs of symmetric/antisymmetric states localized in the  $\mathcal{I}_\pm$  resonance islands (here shown for the “ground state” inside the island). The classical dynamics is fixed at  $\gamma = 0.18$  (compare with figure 2-e). The existence of large fluctuations over several orders of magnitude is a signature of chaos assisted tunnelling. On the average,  $\ln |\Delta\epsilon_n|$  appears to decrease more or less linearly with  $\hbar_{\text{eff}}^{-1}$  except for the plateau at  $15 \leq \hbar_{\text{eff}}^{-1} \leq 30$ ,

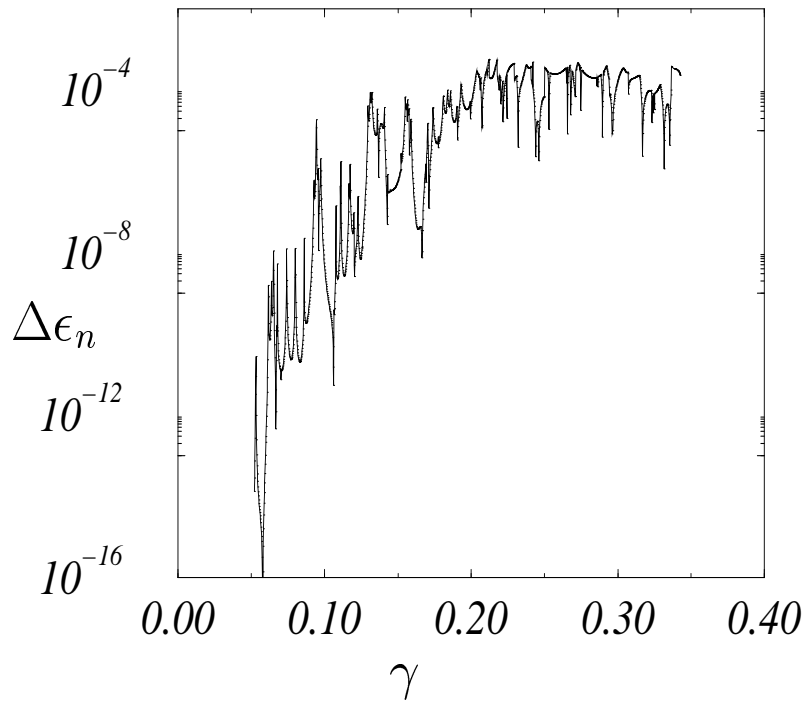


FIG. 8. Fluctuations of the energy splittings  $\Delta\epsilon_n$  between the pair of symmetric/antisymmetric states ( $\hbar_{\text{eff}}^{-1}$  is fixed at 19.309) as a function of  $\gamma$ . Again, the large fluctuations over several orders of magnitude are a signature of chaos assisted tunnelling. The global increase with  $\gamma$  is due to the growth of the chaotic sea as  $\gamma$  increases, see figure 2.



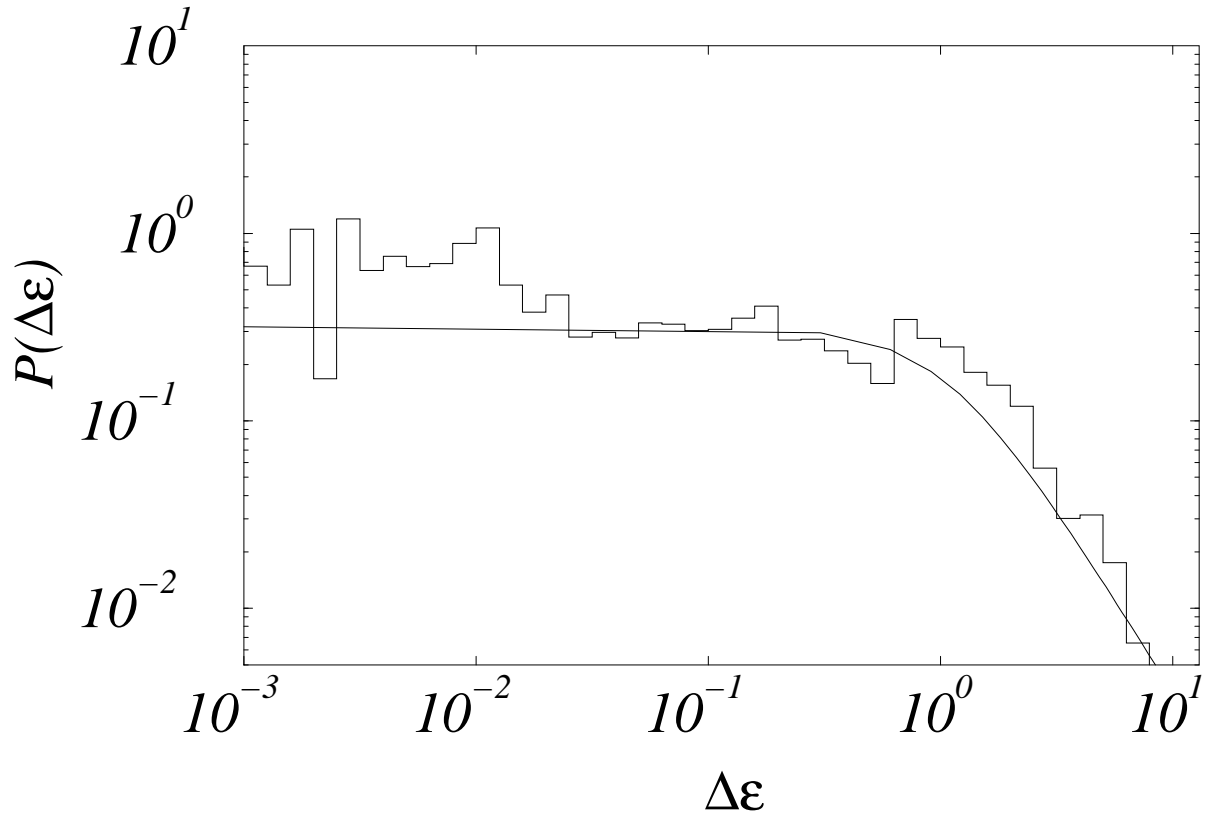


FIG. 9. Statistical distribution of the energy splittings  $\Delta\epsilon$  (normalized to the typical splitting) between pairs of symmetric/antisymmetric states localized inside the  $\mathcal{I}_{\pm}$  resonance islands ( $\gamma = 0.18$ ,  $k = 0$ ), represented on a double logarithmic scale. One can clearly distinguish two regimes: constant at small  $\Delta\epsilon$  followed by a  $1/\Delta\epsilon^2$  decrease and finally a rapid cut-off (not shown in the figure). The solid line is the Cauchy distribution predicted by Random Matrix Theory.

